Modeling of the Thermomechanical Response of Ultrasonically Activated Soft Tissue

By

Congran Jin

A Thesis Submitted to the Graduate
Faculty of Rensselaer Polytechnic Institute
In Partial Fulfillment of the
Requirements for the Degree of

MASTER OF SCIENCE

Major Subject: MECHANICAL ENGINEERING

Approved by the
Examining Committee:

_____
Professor Suvranu De, Thesis Advisor, Chair

_____
Professor Antoinette M. Maniatty, Member

_____
Associate Professor Lucy Zhang, Member

Rensselaer Polytechnic Institute
Troy, New York

April 2016
(For Graduation May 2016)

CONTENTS

LIST OF TABLES

LIST OF FIGURES

ACKNOWLEDGMENTS

First, I would like to express my deepest gratitude to my thesis advisor, Prof. Suvranu De, for giving me the opportunity to work on a practical and challenging problem, for his guidance throughout my thesis, and for the machine and office space he generously offered to me. Also, I would like to give my sincere gratitude to Dr. Rahul who spent a lot of time with me, instructing me on the modeling part of this thesis and helping me with other aspects of my research. Moreover, I would like to give thanks to Prof. De's Ph.D. student Hanglin Ye who patiently answered my numerous questions regarding Abaqus and VUMAT. I would also like to thank members of my thesis committee, Professor Maniatty and Zhang. Last but not the least, I must thank my parents for their continuous support for my education and every decision I have ever made. Without these people, I would not have the chance to present this thesis.

ABSTRACT

A multi-physics computational model has been developed to investigate the thermomechanical response of the ultrasonically activated soft tissue. In pursuit of better understanding of the extent of deformation of soft tissues subjected to harmonic excitations, the cellular level cavitational effect has been incorporated in the tissue level continuum model to accurately determine the thermodynamic states such as temperature and pressure. The cavitation model based equation of state (EOS) captures the additional pressure as a result of evaporation of intracellular and cellular water by absorbing heat due to frictional heating in the tissue, and temperature in the continuum level thermomechanical model. The extent of deformation of the soft tissue is studied for the simulated range of frequencies of harmonic oscillations and applied loads. The model is shown to capture characteristics of ultrasonically activated soft tissue deformation and temperature fields. At the cellular level, evaporation of water below 100°C is indicative of protein denaturation and coagulation much below the boiling temperature under ambient conditions. Further, it is revealed that with the increasing operating frequency and loading, the evaporation of water starts earlier, which may lead to accelerated protein denaturation and coagulation.

1. INTRODUCTION

Ultrasonic surgical instruments have been gaining popularity among surgeons in the last decade. An increasing number of surgical procedures including but not limited to head, neck, gynecological, colorectal surgeries, cholecystectomy, hemoraidectomy, thyroidectomy, tonsillectomy are performed using ultrasonic surgical instruments. These instruments utilize ultrasonic vibrations to cut, coagulate and dissect tissues, and seal vessels. They have been proven to be superior to conventional instruments and techniques such as electrosurgical and laser-based devices as they impose lesser thermal injury, desiccation and charring, lower mean blood loss during surgery, no risk of stray current, neuromuscular stimulation, lesser operation time and post-operative pain, and no smoke during the operation to occlude laparoscopic view.

Despite the increasing popularity of ultrasound-based surgical procedures, the effects of cellular level mechanisms on the thermomechanical response of ultrasonically activated soft tissues have not been understood completely. The purpose of this thesis is to develop a multi-physics computational model to study the effects of cavitation, due to large transient pressure changes, on the thermomechanical response of ultrasonically activated soft tissue.

In Section 1.1, a brief background of ultrasonically activated soft tissue cutting mechanisms along with review of historical perspective of ultrasonically activated scalpel (UAS) have been presented. Finally, major contributions and thesis outline are given in Section 1.2.

1.1 Ultrasonically activated soft tissue

An ultrasonic surgical device or ultrasonically activated scalpel (UAS) uses mechanical vibrations to cut and coagulate soft tissues. UAS consists of a generator, a handpiece, and a blade. The generator, controlled by a microprocessor, provides power to the acoustic system in the hand piece that contains an ultrasonic transducer, which will vibrate at its natural frequency of 55.5 kHz. Then the blade vibrates at this frequency through an extender (length of the extender depends on the particular application of UAS) that is

attached to the transducer. The longitudinal displacement range of the blade is 60 – 100 μm. Devices that operate at frequencies other than 55.5 kHz also exist.

The first reported use of UAS can be traced back to 1960s for treating Meniere's disease (James et al. 1962). Kelman (1967) used ultrasonic energy in an aspiration to remove human tissue. Flamm et al. (1978) concluded that using ultrasonic energy was an effective way of cutting tissue that contains a significant amount of water after studying the effect of ultrasound on spinal cord and cat brain tissue. In the late 1980s, ultrasonic energy was used for cutting and coagulation of tissue. Amaral made use of ultrasonic energy in surgery popular. The technique was proven by him to be effective in cutting and coagulating tissues based on his animal studies (Amaral 1994). It is now widely used in laparoscopic surgeries because of its advantages that are associated with its unique working modes.

There are two primary modes of UAS in dealing with soft tissues: cutting and coagulation. Blood vessels bleed when cut. However, by using the UAS coagulation mode, bleeding can be prevented. The mechanical energy of oscillation is transferred to the tissue in the form of heat (e.g. due to frictional sliding) which increases the temperature of the tissue. The protein in soft tissue will denature at 80°C - 100°C, and when it cools down to 63°C, a sticky coagulum will be formed sealing the blood vessel. In the cutting mode, cavitational effect plays an important role (Lee and Park 1999). The oscillation of the surgical blade will subject the surface of the soft tissue to significant transient pressure change. In the meantime, the temperature will rise as a result of frictional, viscous and deformation heating. At a pressure that is lower than 1atm, the water contained in the tissue will evaporate and rupture the cellular walls at a temperature below 100°C. Therefore, less thermal damage will result compared with other surgical procedures such as electrosurgery and laser ablation which causes the water in the tissue to evaporate at 100°C. In addition to this major benefit of UAS, another advantage is the lack of current transmission, which eliminates the risk of electrical shock. Also, since there is less heat generation, significantly reduced protein charring/desiccation as well as no smoke in the working process, it provides a clear visualization for the laparoscope.

Cavitational effect is considered to be a crucial factor in ultrasonic surgery. Fong et al. (2006) studied the behavior of cavitation bubbles and found that they behave differently in different biomaterials in an ultrasound field. The behavior of cavitation bubbles has not been carefully observed or modeled in the application of UAS. However, Majaron et al. (1999) proposed a microscopic physical model of the explosion of the bubbles or cavities in thermo-mechanical laser ablation of soft biological tissue. Although, this model is not intended for UAS, it provides the background for an equation of state and an energy balance equation at the cellular level.

There are many advantages of UAS, and one of the most important is that UAS works at a lower temperature than electrosurgery. Meltzer et al. (1994) found that the lateral thermal damage by UAS is four times less than that by electrosurgery. Temperature elevation in tissue in the application of UAS was studied by Kock et al. (2003) by using specially designed thermocouples. They compared the temperature elevation at different distance from the blade and found a temperature elevation of 40°C - 50°C at 1 mm distance from the blade. In their experiment, no morphologic indication of thermal damage was found at a distance of more than 2 mm. Besides, Bandi et al. (2008) reported the blade temperature of two harmonic scalpel models at different power levels and the highest temperature they observed was 80.9°C. Even though most researchers assert that the temperature of tissue in the application of UAS will not exceed 100°C, one study has shown that the tip temperature during the activation of harmonic scalpel may rise to 297°C at high power levels and long activation time (Emam and Cuschieri 2003).

Another key advantage of UAS is that it does not require electrical transmission. Due to this characteristic, operations in locations that are near stomach, bowel, or the biliary tree can be performed without the risk of perforation or bile duct injury that plague radiofrequency in electrosurgery (Amaral 1995). Other advantages include that UAS does not produce smoke and thus provides a good visibility and reduces postoperative adhesions (Amaral and Chrostek 1997).

The UAS has disadvantages including longer coagulation times compared with electrosurgery, blade fatigue, temperature elevation, excessively applied pressure and improper use. In addition, ultrasonic energy can cause atomization of fluid, creating a

transient mist, which could be a potential distraction during surgery (Sankaranarayanan et al. 2013). Furthermore, it has been reported in many studies that the ultrasonic devices are not as efficient in sealing medium-to-large-sized blood vessels (Hruby et al. 2007; Clements and Palepu 2007; Harold et al. 2003). Moreover, it is shown that UAS produces even higher temperatures (Emam and Cuschieri 2003; Kim et al. 2008) and is not reliable in sealing vessels larger than 3 mm (Wolfe et al. 1991).

Although, clinical application of UAS has been well documented, the mechanics understanding of the interaction between an ultrasonic device and tissue is limited. The design of ultrasonic devices is done semi-empirically and developed through many iterative test steps. Few studies have focused on the cutting ability of ultrasonic instruments (Wiksell et al. 2000). Factors that affect the scalpel-tissue interaction include, e.g. tissue type, its condition, mode of ultrasonic device, frequency, pressure and tip area (Cimino and Bond 1996).

The goal of this thesis is to develop a multi-physics model that provides equilibrated pressure and temperature to the continuum scale tissue model. Such a model is the first step towards a more quantitative understanding of the effects of harmonic oscillation induced cavitation on the thermomechanical response of soft tissue**.**

1.2 Major contributions and thesis outline

The major contributions of this thesis are outlined in Section 1.2.1 followed by organization of the remainder of the thesis in Section 1.2.2.

1.2.1 Major contributions

- Development of a multi-physics computational model that accounts for the effects of cellular level cavitation mechanism on the thermomechanical response of soft tissue.
- Modeling and simulation of thermomechanical response of the ultrasonically activated soft tissue using cavitation model based equation of state (EOS).
- The modeling has been done in Abaqus/Explicit and cavitation model is incorporated using VUMAT.

1.2.2 Outline of thesis

The thesis is organized as follows. In CHAPTER 2, the mathematical modeling has been introduced. Section 2.1 presents the hyperelastic constitutive relations for the tissue. Section 2.2 discusses the cavitation model in detail. Section 2.3 contains several ways of heat generation including heat generation due to elastic deformation, viscous friction and surface friction.

In CHAPTER 3, the computational model is introduced and discussed. Section 3.1 describes the scalpel and tissue modeling, meshing and their initial and boundary conditions in Abaqus CAE. Then it addresses the selection of tissue property parameters. Section 3.2 discusses the Abaqus user subroutine VUMAT that provides a constitutive relation and the cavitation model for the tissue modeled in Abaqus CAE. A flowchart summarizing the entire model in VUMAT is provided in this section. Section 3.3 document the parameters used in this study.

In CHAPTER 4, results of the simulation are presented. These results include the contour plots for temperature, pressure, boiling temperature and vapor content. Also, plots are provided to compare the response of temperature and vapor content to different operating frequencies and loadings. Discussion of the results, performance and limitation of the model are also included in this Chapter.

In CHAPTER 5, some concluding remarks are provided based on the modeling and simulation of the pre-cutting process using harmonic scalpel. Some possible future studies are also proposed.

2. MATHEMATICAL MODELING

This chapter introduces the mathematical modeling of the interactions of a UAS with soft tissue both at the continuum and microscopic scales. The macroscopic model is presented within the framework of large deformation hyperelasticity. The microscopic cavitation model including an equation of state and an energy balance equation is introduced to describe the vaporization of water in the cells. Finally, heat generation during tissue cutting is discussed which involves thermoelastic heating and heating due to frictional sliding.

2.1 Macroscale tissue mechanical modeling

Soft biological tissues exhibit highly complex mechanical characteristics that can hardly be described by a simple model. The aim of this work is to develop a preliminary understanding of ultrasonic tissue cutting. For the sake of simplicity, we will limit our constitutive modeling to Neo-Hookean hyperelasticity. Extension to other, more accurate and sophisticated, models will be left for future work.

For large deformation elasticity, an appropriate kinematic description of tissue motion is adopted (Bathe 1996) with a Neo-Hookean constitutive model in which the Cauchy stress ($\boldsymbol{\sigma}$) is given by

$$\boldsymbol{\sigma} = \frac{\mu}{J} dev(\overline{\boldsymbol{B}}) + \kappa(J-1)\boldsymbol{I} \tag{1}$$

$$\overline{\boldsymbol{B}} = J^{-2/3}\boldsymbol{B} \tag{2}$$

where J is the determinant of the deformation gradient tensor, μ and κ are material properties, and $\boldsymbol{B}$ is the left Cauchy-Green deformation tensor. The $\kappa(J-1)$ term in equation (1) is also the hydrostatic part of the Cauchy-Green tensor which can be used as pressure in the cavitation model.

2.2 Microscale cavitation model

As explained previously, cavitation plays a crucial role in the cutting process of soft tissue using harmonic scalpel. Majaron et al. (1999) proposed a micro-explosion-based physical model for the thermomechanical laser ablation process by assuming that soft

tissue consists of only two media: a spherical cavity that is initially filled with water and its non-absorbing elastic surrounding. In this work, we have developed a microscale model of tissue cavitation based on that work.

2.2.1 Equation of state

As demonstrated in Figure 1, initially, the cavity (volume V_0) is filled with water at body temperature (T_0=36°C) and the pressure in the cavity is one atmosphere ($P_0 = P_{atm}$= 101,250 Pa). As the blade of the harmonic scalpel oscillates, the mechanical energy is converted to heat (details of the heat generation are discussed in Section 2.3) in the tissue increasing the temperature of the water trapped in the cavity. When the water temperature reaches its boiling point, the water evaporates and further heating converts a fraction of water (x) to vapor which expands and exert pressure on the cavity wall, changing the initial volume (V_0) of the cavity to a new volume (V). Notice that the boiling temperature is not necessarily 100°C due to the transient pressure change in the cavity. As a matter of fact, in the application of harmonic scalpel, the average pressure inside the cavity could be less than one atmosphere, and thus the average boiling temperature for water in the cavity is less than 100°C.

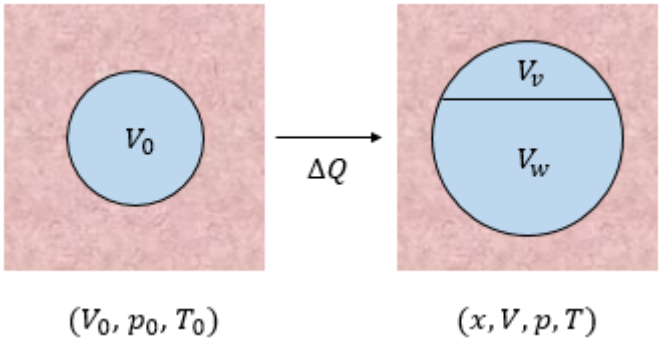

Figure 1. Demonstration of the cavitation model. Heat is added to a spherical cavity initially filled with water surrounded by an infinite elastic medium, resulting in a fraction of water (x) converted to vapor and changes in volume, pressure and temperature.

The new volume (V) has two components: the volume of water (V_w) and the volume of vapor (V_v).

$$V = V_w + V_v = V_0\left[\left(\frac{rT\rho_w}{p} - 1\right)x + 1\right] \tag{3}$$

where T is the current temperature, r is the specific gas constant for water vapor and ρ_w is the density of liquid water which is assumed to remain constant. To derive equation (3) we have used mass conservation:

$$\rho_w V_0 = \rho_w V_w + \rho_v V_v \tag{4}$$

where ρ_v is the density of water vapor, related to the pressure (p) inside the cavity through the ideal gas law:

$$p = \rho_v r T \tag{5}$$

and

$$x = \frac{\rho_v V_v}{\rho_w V_0}. \tag{6}$$

The new volume of the cavity after vaporization depends on the pressure (p) inside the cavity and the mechanical properties of the cavity which follows the relationship for a spherical cavity in an infinite elastic medium (Landau and Lifshitz 1986):

$$V = V_0 \left[1 + \frac{1+v}{2E}(p - p_0)\right]^3 \tag{7}$$

where v is Poisson's ratio, E is Young's modulus and p_0 is the initial pressure in the cavity.

Rearranging equations (3) and (7), we get an expression for the mass fraction (x):

$$x = \frac{\left[1 + \frac{1+v}{2E}(p - p_0)\right]^3 - 1}{\frac{rT\rho_w}{p} - 1}. \tag{8}$$

An analytical formula can be derived from the Clausius-Clapeyron equation to relate temperature and pressure, assuming that the two phases are in thermodynamic equilibrium at all times (Potter and Somerton 1993):

$$\frac{dp}{dT} = \frac{pq(T)}{rT^2} \tag{9}$$

where $q(T)$ is the latent heat of water that is dependent on temperature. This relation can be integrated as

$$\frac{1}{T} = \frac{1}{T_b} - \frac{r}{\bar{q}} \ln\left(\frac{p}{p_0}\right) \tag{10}$$

where $\bar{q}$ is the mean value of the latent heat of water in the temperature interval $[T_0, T]$ and T_b is the boiling temperature which depends on the pressure in the cavity and is determined by Antoinie equation (Stull 1947):

$$T_b = \frac{1435.264}{4.654 - \log(p)} + 64.848 \tag{11}$$

where the units of pressure and temperature in this equation are bars and Kelvin, respectively. By substituting the expression for temperature from equation (10) into equation (8), the following equation of state (EOS) is obtained for the cavity, relating vapor content and pressure:

$$x = \frac{\left[1 + \frac{1+v}{2E}(p - p_0)\right]^3 - 1}{\frac{r\rho_w T_b \bar{q}}{p(\bar{q} - rT_b \ln(p/p_0))} - 1}. \tag{12}$$

2.2.2 Energy balance equation

In the application of UAS, the local thermodynamic variables change as a result of heat addition to the tissue, and therefore the following energy balance equation may be written:

$$\Delta Q = \Delta H_{evp} + \Delta Q_{vap} + \Delta Q_{wat} + \Delta Q_{sol} + \Delta W_{sur} \tag{13}$$

where ΔQ (J/m^3) is heat addition density and has five components: the enthalpy change in additional evaporation (ΔH_{evp}), the heating of vapor (ΔQ_{vap}), the heating of water (ΔQ_{wat}), the final conductive thermalization of the solid part within the cavity (ΔQ_{sol}) and the work done on the surrounding tissue (ΔW_{sur}).

ΔH_{evp} can be expressed as:

$$\Delta H_{evp} = \rho w q(T) \Delta x \tag{14}$$

where ρ is the average density of the tissue, w is the water content in the cavity. ΔQ_{vap} can be expressed as:

$$\Delta Q_{vap} = \rho w x (c_v + r)\Delta T \tag{15}$$

where c_v is the specific heat capacity of vapor. ΔQ_{wat} can be expressed as:

$$\Delta Q_{wat} = \rho w (1 - x) c_w \Delta T \tag{16}$$

where c_w is the specific heat capacity of vapor. ΔQ_{sol} can be expressed as:

$$\Delta Q_{sol} = \rho (1 - w) c_s \Delta T \tag{17}$$

where c_s is the specific heat capacity of the solid surroundings. Finally, ΔW_{sur} can be expressed as:

$$\Delta W_{sur} = -\rho \frac{w \Delta p}{\rho_w}. \tag{18}$$

Now equation (13) can be expressed as:

$$\begin{aligned} \Delta Q = \rho [& w q(T) \Delta x + w x (c_v + r)\Delta T + w(1 - x) c_w \Delta T \\ & + (1 - w) c_s \Delta T - w \Delta p / \rho_w] \end{aligned} \tag{19}$$

The energy balance equation combined with the equation of state gives a highly nonlinear set of equations. To solve the set of equations, Δx is replaced by $(dx/dT)\Delta T$ and Δp by $(dp/dT)\Delta T$ and equation (19) can be solved for ΔT:

$$\Delta T = T - T_0 = \frac{\Delta Q}{\rho w \left[q(T) \frac{dx}{dT} - (c_w - c_v - r)x + c_w + \frac{1 - w}{w} c_s - \frac{1}{\rho_w} \frac{dp}{dT} \right]} \tag{20}$$

where T is the current temperature and T_0 is the temperature from previous time step in our simulation, and dx/dT can be derived from equation (8):

$$\begin{aligned} \frac{dx}{dT} = & \frac{\frac{3(1 + v)}{2E} \left[1 + \frac{(1 + v)(p - p_0)}{2E} \right]^2 \frac{dp}{dT}}{\frac{rT\rho_v}{p} - 1} \\ & - \frac{\left\{ \left[1 + \frac{(1 + v)(p - p_0)}{2E} \right]^3 - 1 \right\} \frac{rT\rho_v}{p} (1 - \frac{T}{p} \frac{dp}{dT})}{(\frac{rT\rho_v}{p} - 1)^2} \end{aligned} \tag{21}$$

where the derivative dp/dT is given by equation (9). In our simulation the current temperature T is solved numerically by using Newton's method.

2.3 Heat generation and temperature evolution

In the application of UAS, the temperature of the tissue rises due to heat addition to the tissue. As the blade vibrates, part of the mechanical energy of the vibration is converted to heat in three ways: thermoelastic deformations, viscosity and frictional heating at the interface of the scalpel and the tissue. The total heat addition (ΔQ) to the tissue has, therefore, three components, thermoelastic heating (ΔQ_{el}), viscous heating (ΔQ_{vi}) and frictional heating (ΔQ_{fr}):

$$\Delta Q = \Delta Q_{el} + \Delta Q_{vi} + \Delta Q_{fr}. \tag{22}$$

Moreover, the total heat addition and temperature difference (ΔT) of the tissue are related by the following relationship:

$$\Delta Q = \Delta T \rho c_s \tag{23}$$

where c_s is the specific heat of the tissue and ΔT is the equilibrium temperature change between the current step and the previous step $\Delta T = T_n - T_{n-1}$. In this work, we will neglect the effect of viscous heating and consider only from thermoelastic and frictional sources.

2.3.1 Elastic deformation heating

Elastic deformation will create heat in the tissue and the temperature evolution follows the relationship:

$$T_n = T_{n-1} \exp\left(-\frac{1}{2}\boldsymbol{\gamma} : \Delta \boldsymbol{C}\right). \tag{24}$$

Here ΔC is the change in the right Cauchy-Green tensor between the current step and previous step and γ is the Grüneisen tensor (Wallace 1972) which can be expressed as:

$$\boldsymbol{\gamma} = \frac{\boldsymbol{L} : \boldsymbol{\beta}}{\rho c_p} \tag{25}$$

where $\boldsymbol{L}$ is the 4th order elasticity tensor and $\boldsymbol{\beta}$ is the coefficient of thermal expansion of soft tissue. Note that the effect of this heating vanishes over a complete vibration cycle and is not considered in the simulation.

2.3.2 Frictional heating

Another heat source comes from frictional sliding on the interface of the scalpel blade and tissue surface. In our simulation, the heat due to frictional sliding is calculated using Abaqus provided that the contact property is properly defined. In Abaqus' coupled thermal-mechanical surface interactions, the rate of frictional energy dissipation (P_{fr}) is given by

$$P_{fr} = \boldsymbol{\tau} \cdot \dot{s} \tag{26}$$

where $\boldsymbol{\tau}$ is the frictional stress and $\dot{s}$ is the slip rate. The frictional stress depends on the contact pressure and the friction coefficient. The amount of energy that is released as heat to scalpel and tissue is assumed to be

$$q_{scalpel} = f\eta P_{fr} \tag{27}$$

and

$$q_{tissue} = (1 - f)\eta P_{fr} \tag{28}$$

where η is the fraction of dissipation energy that transfers to heat and f is the fraction of the generated heat in the scalpel. These quantities should be empirically derived, but in our simulation, we assumed that η is 0.9 and f is 0.6.

3. COMPUTATIONAL MODELING

This chapter presents the computational model employed in the simulation. In the beginning, the thermal-stress analysis used in the commercial finite element software package Abaqus/Explicit is briefly recapitulated. Then the 3-D modeling of scalpel and tissue, meshing method as well as initial and boundary conditions are described. Thereafter, the Abaqus user-subroutine for the cavitation model is discussed. Finally, some relevant parameters used in the simulation are summarized in a table.

3.1 Thermal-stress analysis

Abaqus/Explicit is a finite element analysis software package that is a part of Abaqus by SIMULIA for simulating transient dynamic events such as the UAS oscillation and its interaction with soft tissue in our case.

In fully coupled thermal-stress analysis in Abaqus/Explicit, the heat transfer equation is integrated using the explicit forward difference time integration rule:

$$\theta_{i+1}^{N} = \theta_{i}^{N} + \Delta t_{i+1}\dot{\theta}_{i}^{N} \tag{29}$$

where θ^N is the temperature at node N, and the subscript denotes the increment number in an explicit dynamic step. The forward-difference integration is explicit in that when a lumped capacitance matrix is used, no equations need to be solved. $\dot{\theta}_i^N$, from the previous step, is calculated at the beginning of the current step by

$$\dot{\theta}_{i}^{N} = (C^{NJ})^{-1}(P_{i}^{J} - F_{i}^{J}) \tag{30}$$

where C^{NJ} is the lumped capacitance matrix, P^J is the applied nodal source vector, and F^J is the internal flux vector. The stress response is obtained using the explicit central-difference integration rule with a lumped mass matrix. Because both the forward-difference and central-difference integration are explicit, the thermal and stress problems are solved simultaneously by an explicit coupling.

3.1.1 Parts and meshing

In Abaqus CAE, we consider a model consists of two parts (Figure 2). The upper part is a $2\times9.5\times1\ mm^3$ block representing the blade of the UAS and the lower part is a 4×4×

$2\ mm^3$ block representing a soft tissue sample with homogeneous properties. Notice that the area of the bottom face of the blade is similar to that of a real UAS blade. The blade is assumed as a rigid body. However, the tissue block has been assigned a material model including a constitutive relation and the cavitation model that is defined in a user-subroutine VUMAT.

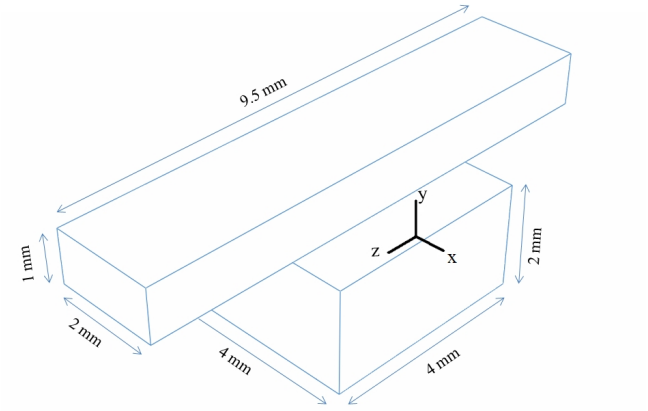

Figure 2. Scalpel blade and tissue block model.

The blade is meshed only with two elements because it is a rigid body, and the tissue is meshed with 2,048 quadratic hexahedral elements (Figure 3).

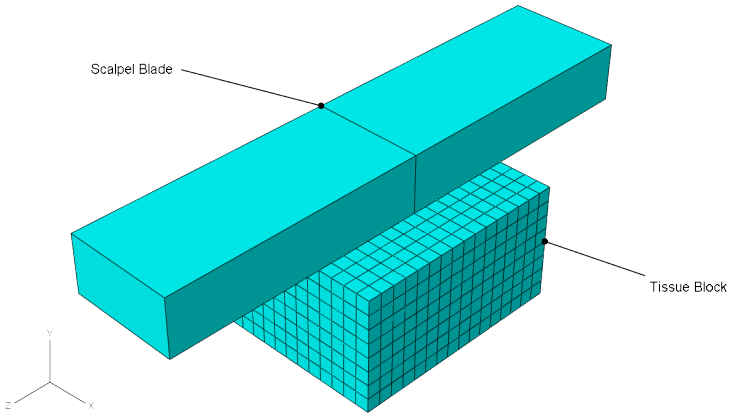

Figure 3. Mesh for scalpel blade and tissue block.

3.1.2 Initial and boundary conditions

The initial temperature of both the tissue block and the scalpel is set to the body temperature (37°C). There are three boundary conditions. The first boundary condition fixes degree of freedom in x, y and z directions of the middle part of the bottom face of

the tissue block to simulate the jaws of the scalpel that clutches the tissue and prevent it from moving around. The second boundary condition is a sinusoidal displacement boundary condition applied to the blade:

$$u = u_0 \sin(\omega t) \tag{31}$$

where u is the displacement, u_0 is the amplitude of the displacement and ω is the frequency of the oscillation. In our simulation, u_0 is 100 μm and four values for ω has been used: 35 kHz, 55 kHz, 75 kHz and 95 kHz.

The third boundary condition is also a displacement boundary condition that specifies the displacement of the scalpel in the direction that is normal to the tissue surface (in y direction). This boundary condition can be considered as loading of the scalpel since it controls how "deep" the scalpel blade goes and it produces equivalent effect on the tissue as the loading does. Three different values for this displacement are used in the simulation: 0.08 mm, 0.1 mm and 0.12 mm.

3.2 VUMAT

VUMAT is a user-subroutine for Abaqus/Explicit that provides material properties, constitutive relations and other mechanical characteristics. In Abaqus/Explicit the user-defined material model is implemented in a user subroutine VUMAT.

Initially, the pressure in the cavity is assumed as one atmosphere pressure (P_{atm}=101,325 Pa), and the temperature is at human body temperature (37°C). Since there is no vaporization at this point, the vapor fraction x is 0.

The pressure is updated by the following equation:

$$P = |P_{atm} - Hyd| \tag{32}$$

where Hyd is the hydrostatic part of the stress tensor ($\boldsymbol{\sigma}$) which is determined by:

$$Hyd = \frac{1}{3}(\sigma_{11} + \sigma_{22} + \sigma_{33}) \tag{33}$$

where σ_{11}, σ_{22} and σ_{33} are the diagonal entries of the stress tensor, or in the neo-Hookean hyperelastic model, it can also be determined by the second term of equation (1).

The temperature is obtained directly from Abaqus due to frictional sliding, while the boiling temperature is calculated using equation (11). If the temperature is higher than the boiling temperature, one situation needs to be excluded before the model goes into the cavitation part that is: heat addition is less or equal to zero and vapor content is zero. Negative heat addition with the existence of some vapor means that the vapor will condense back to water in the cavity, so negative heat without vapor should not be allowed in the cavitation model. Then the updated temperature, pressure and vapor content are computed. Figure 4 shows the flowchart of the model in VUMAT, which is written in Fortran 77.

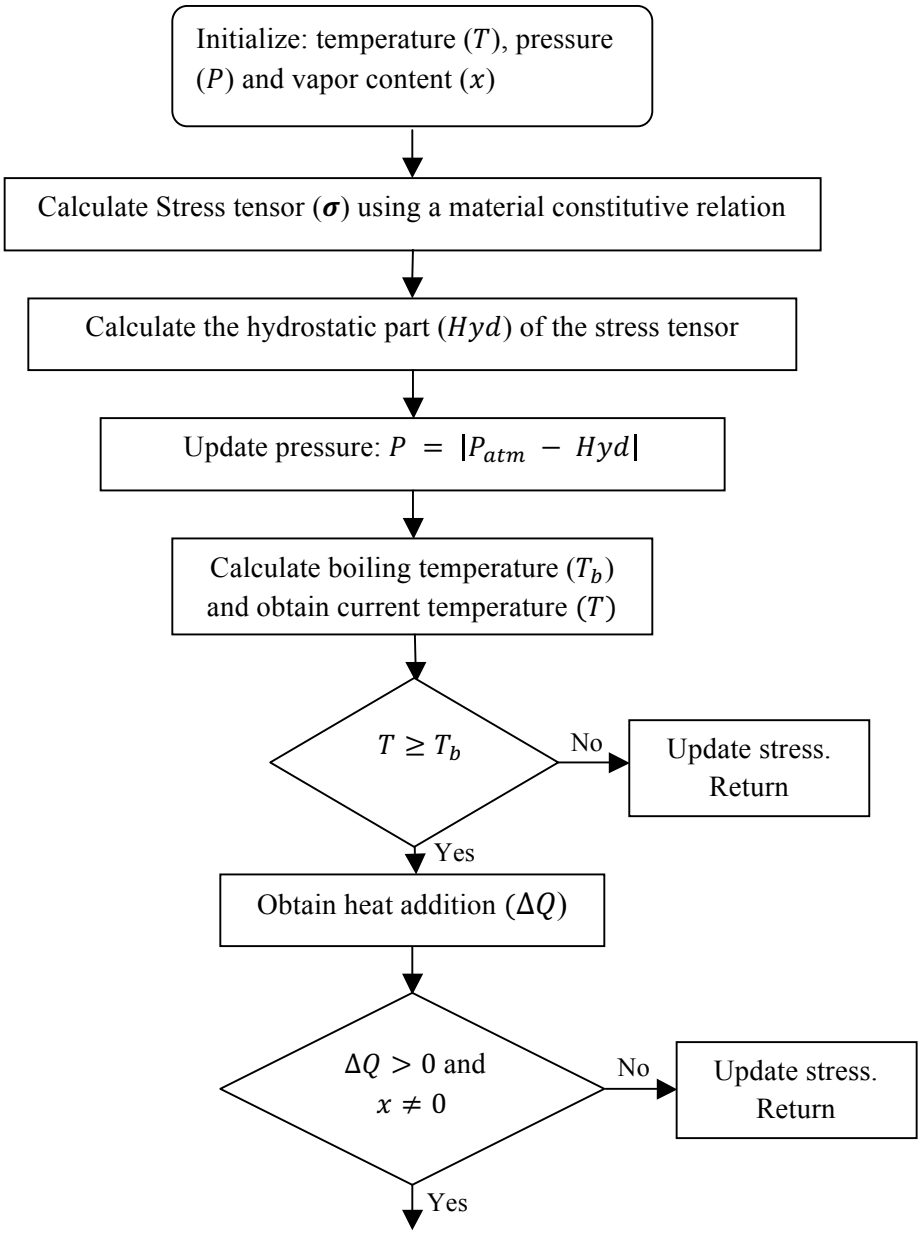

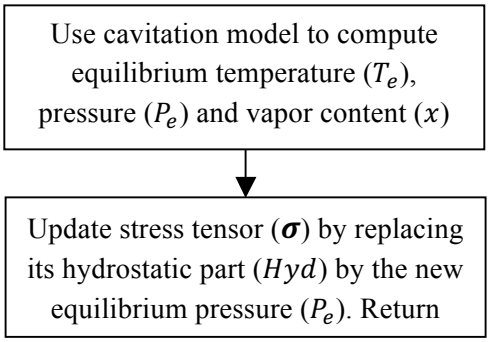

Figure 4. Flowchart of VUMAT model.

3.3 Parameters

Tissue may be classified as hard tissue such as bone and soft tissue including tendons, ligaments, fascia, skin, muscles, fibrous tissues, nerves, connective tissues, and blood vessels. Different types of soft tissue possess different physical parameters. In this thesis, an average value of each parameter is used because, instead of showing and comparing the responses corresponding to different types of tissues, the intent of this thesis is to provide a starting point that captures the basic properties of soft tissues with a relatively high water content. The following table summarizes the parameters used for the simulation.

Table 1. Some parameters used in the simulation.

Name	Value	Unit
Young's modulus (E)	500,000	Pa
Poisson's ratio (υ)	0.49	
Average density (ρ)	1100	$Kg.m^{-3}$
Water content (w)	70%	
Water part density (ρ_w)	943	$Kg.m^{-3}$
Vapor part density (ρ_v)	150	$Kg.m^{-3}$
Avg. specific heat capacity (c_p)	3390	$J.kg^{-1}.K^{-1}$
Specific heat capacity of solid part (c_s)	1700	$J.kg^{-1}.K^{-1}$
Specific heat capacity of water part (c_w)	4248	$J.kg^{-1}.K^{-1}$
Specific heat capacity of vapor part (c_v)	1930	$J.kg^{-1}.K^{-1}$
Specific Gas constant for water vapor (r)	462	$J.kg^{-1}.K^{-1}$
Coefficient of thermal expansion (α)	0.0001	$°C^{-1}$
Coefficient of friction of tissue	5	
Thermal conductivity	0.3	$W.mK^{-1}$
Atmosphere pressure	101,250	Pa
Initial tissue temperature	36	°C

4. RESULTS AND DISCUSSION

This chapter presents results of the simulation, which is followed by discussions. The thermomechanical responses of ultrasonically activated tissue are first shown in Section 4.1 using contour plots of the simulated tissue block. The evolution of pressure, temperature, and vapor content at an integration point of the specimen is discussed in Section 4.2. In addition, effects of harmonic oscillation frequencies and loading on the thermodynamic states and vaporization of intracellular and cellular water is discussed in Section 4.3 and 4.4, respectively.

4.1 Thermomechanical response

The stress, temperature, pressure and vapor content contours with 55 kHz oscillation frequency and 0.12 mm loading are obtained at 4.2 ms from Abaqus CAE visualization module with the scalpel blade hidden (Figure 5-9). The stress response is shown in Figure 5, where the Von Mises stress distribution is plotted. It can be seen that the peak stress develops at the contact of the scalpel blade with the tissue block on the compressive side of the tissue. The temperature contour plot (Figure 6) shows that the temperature ranges approximately from 37°C (310 K) to 190°C (464 K), where the peak temperature is localized along the farther end edge. The reason for the localization of the temperature is that as the scalpel blade oscillates, it produces tensile and compressive loading in the direction of the motion of the scalpel, and at this moment, the farther side is under compressive loading with more contact between the blade and the tissue element. Therefore, the temperature rises much quicker at the farther edge. Because of the cyclic nature of the loading, the net effect of heat generation will be zero, as pointed out in the previous section.

The pressure contour plot (Figure 7) ranges approximately from 0.488 atm (48,800 Pa) to 3.12 atm (312,000 Pa). Again, the farther side is undergoing compressive loading, so the pressure is high in that region while the nearer side is undergoing tensile loading, so the pressure is lower in this region.

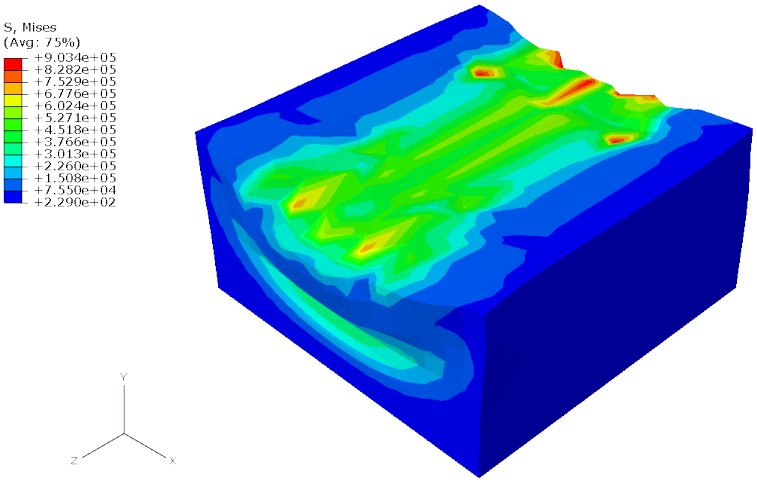

Figure 5. Von Mises stress contour.

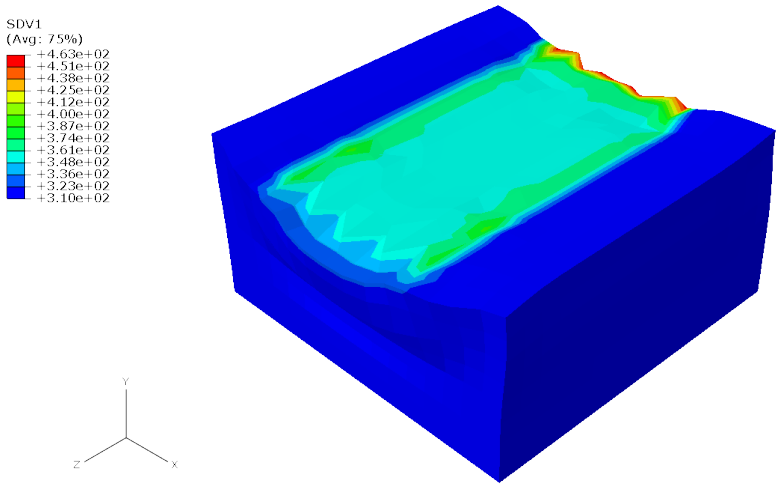

Figure 6. Temperature contour.

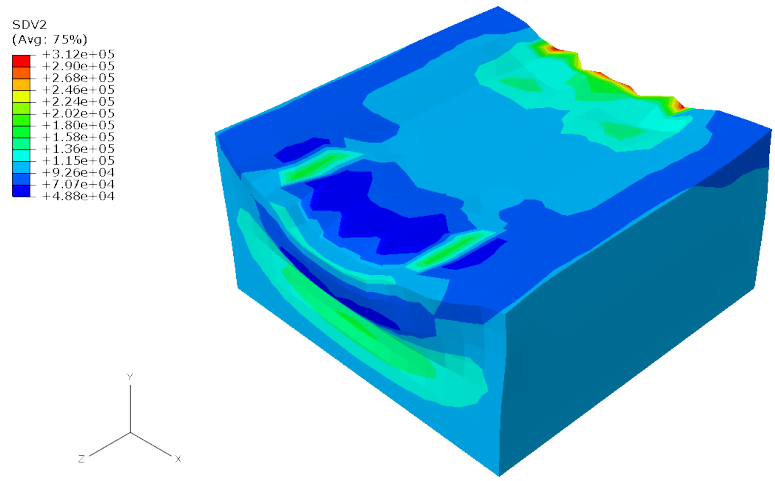

Figure 7. Pressure contour.

Boiling temperature is related to the pressure by Antoinie equation (equation (11)). The boiling temperature contour plot (Figure 8) shows that the yellow area has a boiling temperature that is approximately 100°C (372 K) which is the boiling temperature at one atmospheric pressure. On the top surface of the tissue block, since the farther side is in compression under greater pressure, the boiling temperatures are greater than 100°C. However, on the nearer side, boiling temperatures are lower than 100°C.

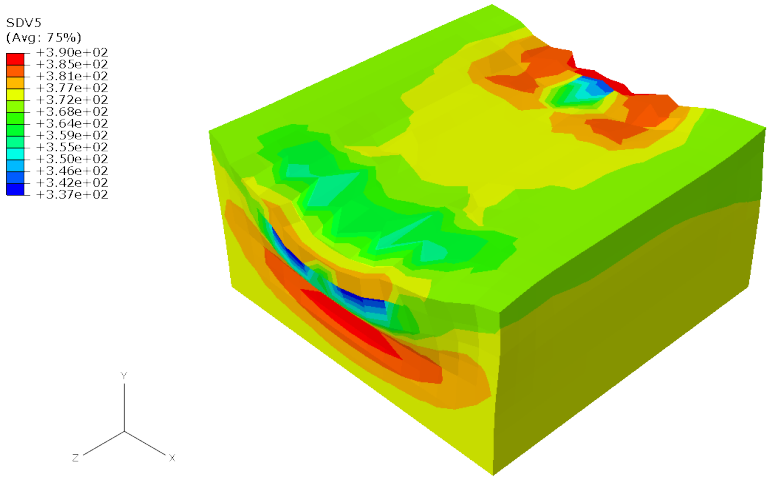

Figure 8. Boiling temperature contour.

The vapor content contour plot (Figure 9) exhibits the vapor content (fraction of water that evaporates) distribution on the tissue block. At this moment, the water starts to vaporize and reach as high as 0.12%. It is observed that the vaporization begins at two regions (the farther side and the nearer side) at the top surface of the tissue block. On the farther side, the water evaporates at higher temperatures. On the nearer side, the boiling temperature ranges from approximately 64°C to 100°C (Figure 8), and the phenomenon is similar to what most research paper assert: in the application of UAS, water evaporates at a boiling temperature less than 100°C and thus create less heat damage to the tissue. Furthermore, the start of water evaporation of approximately 0.02% vapor content is seen on this side. However, due to the localization of heat on the other side of the tissue block, the vaporization phenomenon is not dominating on this side.

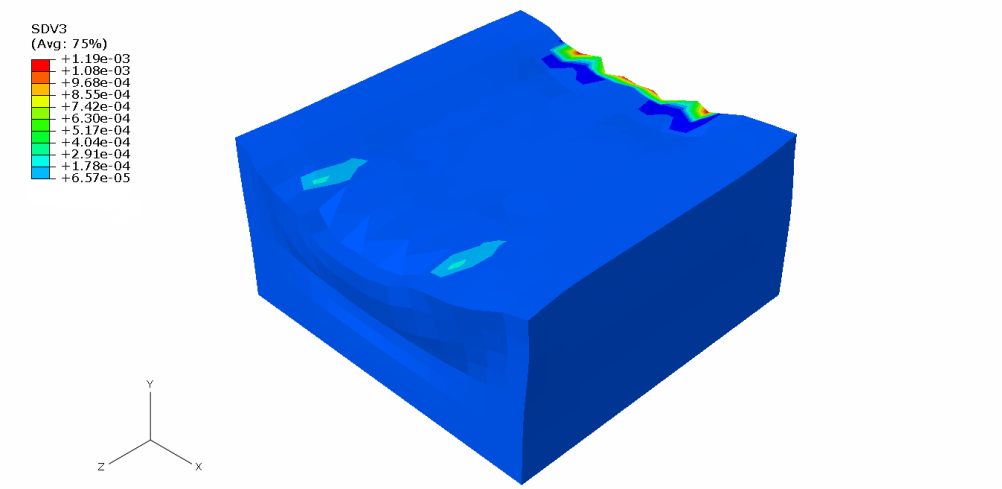

Figure 9. Vapor content contour.

4.2 Evolution of temperature, pressure, vapor content

One element on the top surface near the tensile side of the tissue block is chosen to show the characteristics of water vaporization with a frequency of 55 kHz and a loading of 0.12 mm. In Figure 10, the evolution of temperature, pressure, and vapor content is plotted at the spatial coordinate (0.625 mm, 1.875 mm, 3.375 mm). In the cavitation model, the equilibrium pressure and vapor content are calculated by equation (10) and (8), respectively. The temperature is provided by the displacement-temperature formulation of Abaqus/Explicit and boiling temperature is determined by equation (11). Figure 10(a) provides the temperature and boiling temperature variation with respect to time. Figures 10(b) and 10(c) show the pressure, and vapor content variation with time.

Initially, the boiling temperature (Figure 10(a)) is at 100°C at one atmosphere pressure (Figure 10(b)). Then pressure changes due to the deformation of the element (equation (32) and (33)) and therefore boiling temperature changes. At approximately 3 ms, the pressure drops down to 1 atm and thus boiling temperature drops below 100°C. The temperature starts at body temperature (37°C). As the scalpel starts acting on the tissue, the tissue temperature rises to 78°C, exceeding the boiling temperature of water. This results in vaporization of water below 100°C, indicating cavitation initiation. The tissue temperature continues to increase due to frictional heating for the remainder of the time interval. Between approximately 4 ms and 4.7 ms, water continues to vaporize and the vapor content reaches 0.05% (Figure 10(c)). However, at 4.7 ms, the loading of the

cavity is changed from tensile to compressive, leading to an increase of pressure and boiling temperature. Although the cavity temperature is still increasing after 4.7 ms, the pressure increases at a much higher rate, resulting in condensation of the vapor. Thus, the vapor content starts to decrease after 4.7 mm and gets closer to 0 when the boiling temperature curve nearly intersects the cavity temperature curve at 6 ms.

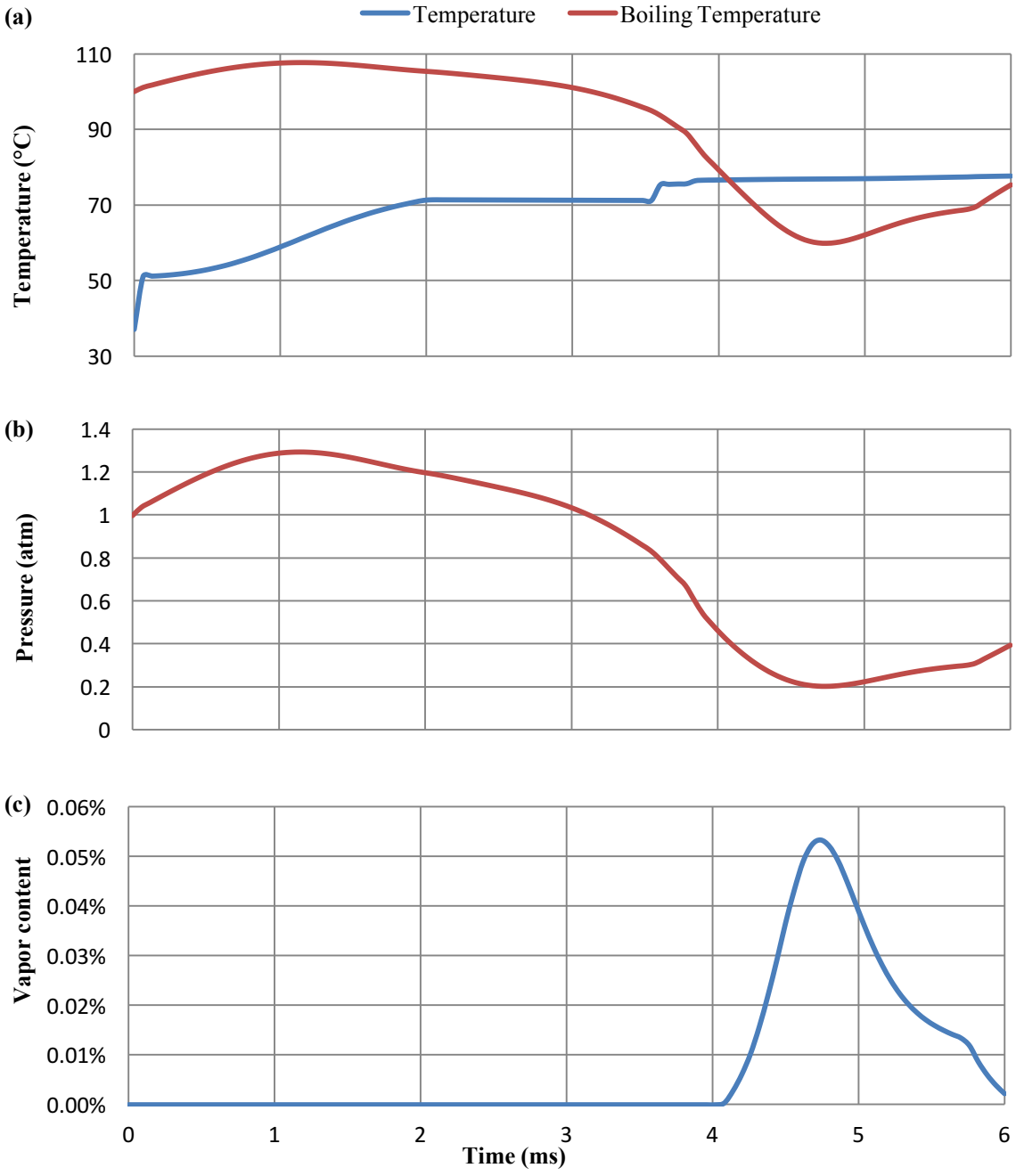

Figure 10. Evolution of temperature, pressure and vapor content. (a) Temperature and boiling temperature vs. time. (b) Pressure vs. time. (c) Vapor content vs. time.

4.3 Effect of harmonic oscillation frequency

The effect of oscillation frequency of the UAS on the temperature of the top surface of the tissue block and the vaporization of water in the cavity is studied in this section. Four different frequencies, 35 kHz, 55 kHz, 75 kHz and 95 kHz, are used to obtain temperature versus time plot (Figure 11(a)), and vapor content versus time plot (Figure 11(b)) on one element at the top surface in the compressive region of the tissue block at spatial coordinate (0.625 mm, 1.875 mm, 0.125 mm) with a loading of 0.12 mm. Temperature is obtained from Abaqus/Explicit displacement-temperature formulation while the vapor content data is obtained from the cavitation model that is written in VUMAT.

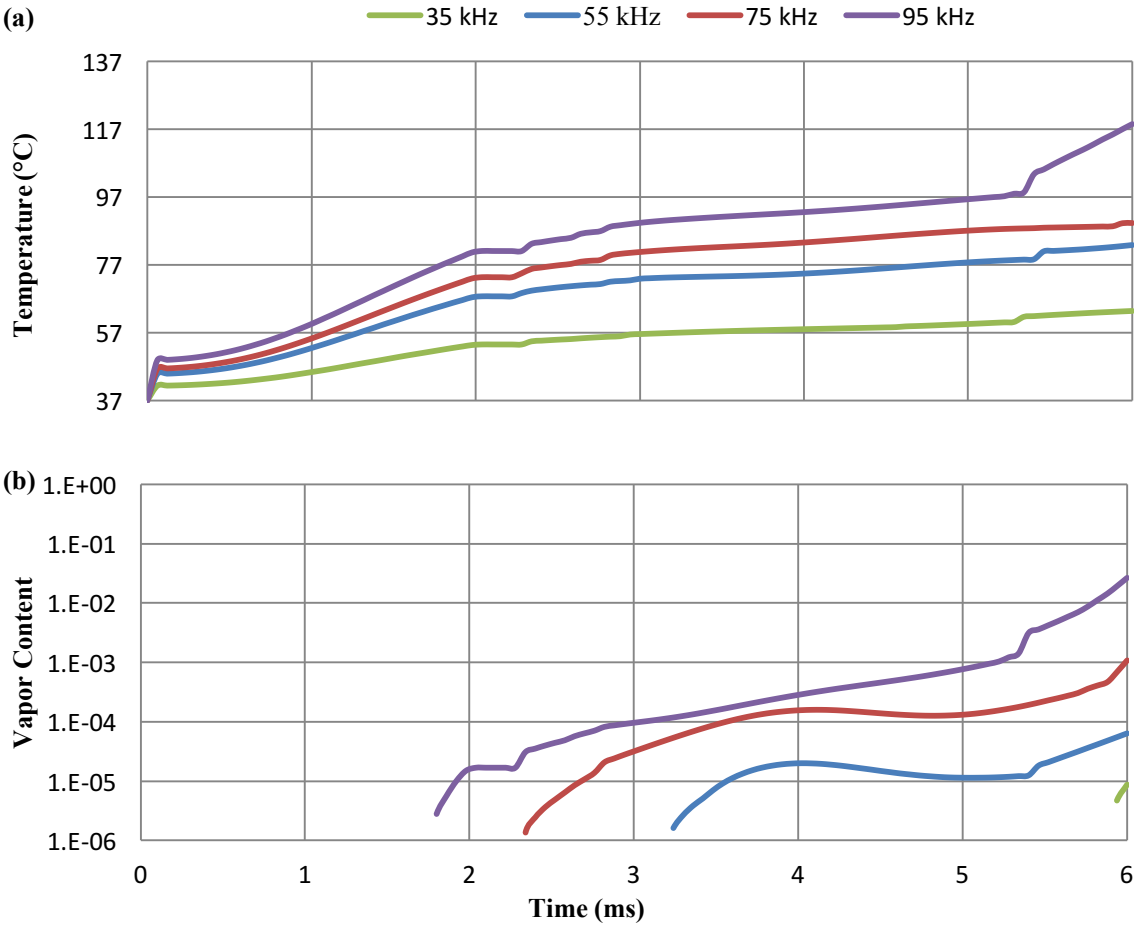

Figure 11. Evolution of temperature and vapor content with different frequencies. (a) Temperature vs. time with different frequencies. (b) Vapor content vs. time with different frequencies.

Figure 11(a) shows that as the frequency increases the temperature rises faster and finally reaches a higher temperature. For example, at 6 ms, tissue temperatures corresponding to excitations at 35 kHz, 55 kHz, 75 kHz and 95 kHz are 63°C, 83°C, 89°C and 119°C, respectively. With increasing frequency, the scalpel blade has more frictional sliding with the surface of the tissue. Essentially, the scalpel with higher frequency interacting with tissue will generate more heat through friction, result in faster temperature rise.

Figure 11(b) exhibits the curve for vapor content (on $\log_{10}$ scale) versus time at different frequencies. As the frequency increases, vaporization of water starts earlier. For example, the time points that water in the cavity starts to vaporize corresponding to excitation at 35 kHz, 55 kHz, 75 kHz and 95 kHz are 5.9 ms, 3.2 ms, 2.3 ms and 1.8 ms, respectively. This is due to the faster temperature rise that accompanies higher frequencies.

4.4 Effect of loading

When the UAS is applied on the soft tissue, other than the oscillation in the direction of motion of scalpel, another load that is normal to the blade-tissue interaction surface is applied to the tissue as well. In our simulation, the loading is defined in terms of the displacement of the scalpel blade. To study the effect of how different loading changes the temperature evolution, three different prescribed displacements are chosen: 0.08 mm 0.1 mm and 0.12 mm. One element on the top surface of the compressive region of the tissue block is chosen to show the evolution of temperature and vapor content at a frequency of 55 kHz in Figure 12(a) and (b), respectively. Plots are obtained at the spatial coordinate (0.375 mm, 1.875 mm, 0.125 mm).

Figure 12(a) shows that as the loading increases, the temperature rises faster, finally reaching a higher temperature. With higher loading, the normal force between the scalpel blade and the tissue surface increases, leading to a higher heat generation due to friction. Therefore, the temperature will rise much faster. Figure 12(b) exhibits the curve for vapor content (in percentage) versus time at different loading. Vaporization of water starts earlier with increased loading. For example, the time that water in the cavity starts

to vaporize for 0.08mm, 0.1mm, and 0.12mm prescribed displacement are 5.3 ms, 3.5 ms and 2.3 ms, respectively.

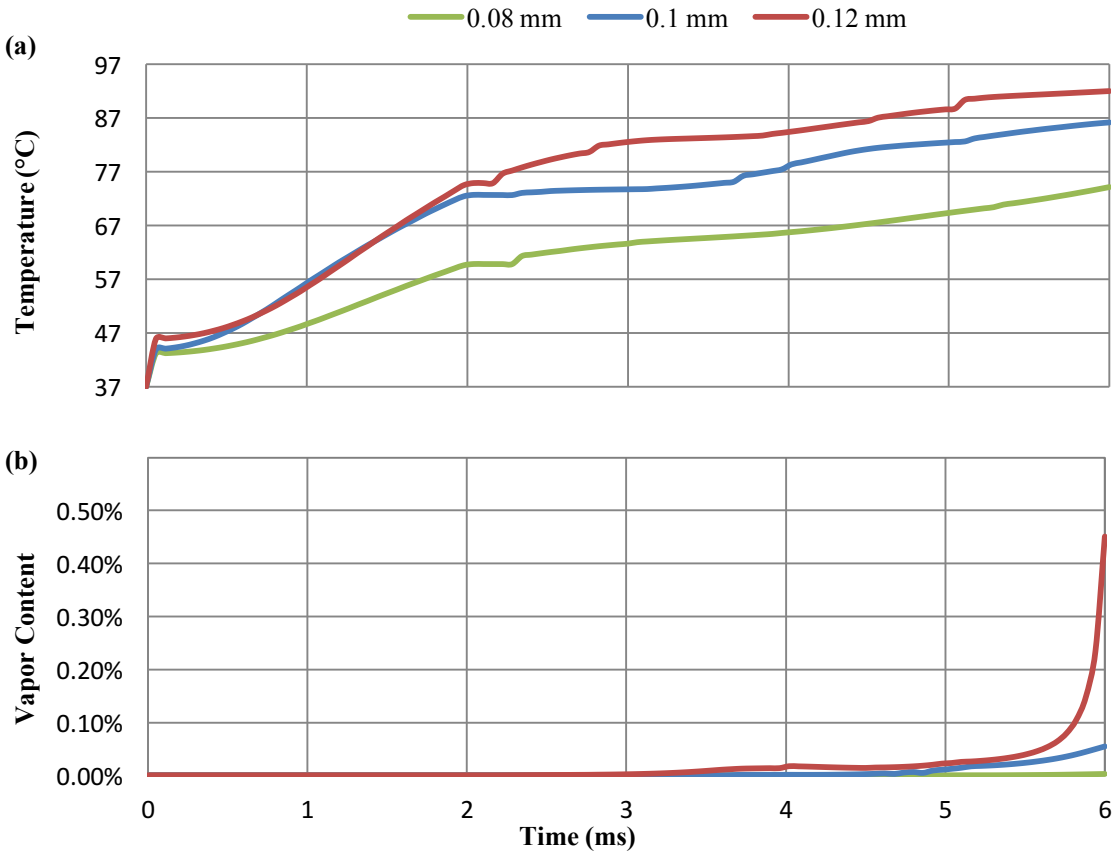

Figure 12. Evolution of temperature and vapor content with different loadings. (a) Temperature vs. time. (b) Vapor content vs. time.

5. CONCLUDING REMARKS

We summarize our work in the first section, followed by a discussion of the limitations of the model and future work in the next section.

5.1 Summary

A multi-physics computational model that includes the cellular level cavitation effect is proposed to describe the thermomechanical response of ultrasonically activated soft tissue. A displacement-temperature finite element analysis is performed using the commercial software package Abaqus/Explicit to simulate the process. The hyperelastic constitutive model and cavitation model are incorporated using VUMAT user subroutine. The evolution of thermodynamic states such as pressure, temperature, and characteristics of vaporization of water (vapor content) of the tissue are studied for a range of oscillation frequencies and loading conditions.

The model is shown to successfully capture characteristics of ultrasonically activated soft tissue deformation and temperature fields as well as vaporization of water below ambient boiling temperature. The contour plots show localization of temperature and vapor content. In fact, it is found that water evaporates at a low temperature (e.g. below 80°C) due to a lowered pressure that is caused by tensile loading on the cavity and at a high temperature (e.g. above 100°C) at a location with compressive loading. It is observed that the higher the frequency of oscillation of the surgical tool, the faster the temperature rise in the tissue and the earlier water starts to vaporize. Another interesting observation is that higher loading, which corresponds to greater grasping force on the tool, leads to faster temperature rise and accelerated water vaporization. Early evaporation of water may be hypothesized to lead to accelerated protein denaturation and coagulation leading to precise cutting and fragmentation of tissue. This observation remains to be validated though experimentation.

5.2 Future work

There are some limitations of the simulation in this thesis. First of all, the coefficient of friction used in the simulation is estimated from literature which might not be realistic in the application of UAS. To capture the actual coefficient of friction, an experiment

designed for finding the real coefficient of friction of UAS and soft tissue interaction needs to be performed. Secondly, the current simulation only shows the state of tissue prior to failure. In other words, there is no damage model that can accounts for the degradation in stiffness due to cellular rupture even if the stress is beyond the elastic limit. For a more complete description of the degradation process, a damage model needs to be employed. Thirdly, the only heat source in the simulation comes from frictional sliding. Nevertheless, viscous heating might be a major contributor of the heat addition to the tissue in reality as well which is currently outside the scope of this thesis. Finally, excessive distortion of elements is likely to occur for longer simulation.

REFERENCES

Amaral, Joseph F. 1994. “The Experimental Development of an Ultrasonically Activated Scalpel for Laparoscopic Use.” *Surgical Laparoscopy Endoscopy & Percutaneous Techniques* 4 (2): 92–99.

———. 1995. “Laparoscopic Cholecystectomy in 200 Consecutive Patients Using an Ultrasonic Activated Scalpel.” *Surgical Laparoscopy Endoscopy & Percutaneous Techniques* 5 (4): 255–62.

Amaral, Joseph F., and Cynthia A. Chrostek. 1997. “Experimental Comparison of the Ultrasonically-Activated Scalpel to Electrosurgery and Laser Surgery for Laparoscopic Use.” *Minimally Invasive Therapy & Allied Technologies* 6 (4): 324–31.

Bandi, Gaurav, Charles C. Wen, Eric A. Wilkingson, Sean P. Hedican, Timothy D. Moon, and Stephen Y. Nakada. 2008. “Comparison of Blade Temperature Dynamics after Activation of Harmonic Ace Scalpel and the Ultracision Harmonic Scalpel LCS-K5.” *Journal of Endourology* 22 (2): 333–36.

Bathe, Klaus J. 1996. *Finite Element Procedures*. New Jersey: Prentice-Hall.

Cimino, William W., and Leonard J. Bond. 1996. “Physics of Ultrasonic Surgery Using Tissue Fragmentation.” *Ultrasound in Medicine & Biology* 22 (1): 89–100.

Clements, Ronald H., and Rajendra Palepu. 2007. “In Vivo Comparison of the Coagulation Capability of SonoSurg and Harmonic Ace on 4-Mm and 5-Mm Arteries.” *Surgical Endoscopy* 21 (12): 2203–6.

Emam, Tarek A., and Alfred Cuschieri. 2003. “How Safe Is High-Power Ultrasonic Dissection.” *Annals of Surgery* 237 (2): 186–91.

Flamm, Eugene S., Joseph Ransohoff, Dave Wuchinich, and Allen Broadwin. 1978. “Preliminary Experience with Ultrasonic Aspiration in Neurosurgery.” *Neurosurgery* 2 (3): 240–45.

Fong, Siew W., Evert Klaseboer, Cary K. Turangan, Boo C. Khoo, and Kin C. Hung. 2006. “Numerical Analysis of a Gas Bubble near Bio-Materials in an Ultrasound Field.” *Ultrasound in Medicine & Biology* 32 (6): 925–42.

Harold, K. L., H. Pollinger, B. D. Matthews, K. W. Kercher, R. F. Sing, and B. T. Heniford. 2003. “Comparison of Ultrasonic Energy, Bipolar Thermal Energy, and Vascular Clips for the Hemostasis of Small-, Medium-, and Large-Sized Arteries.” *Surgical Endoscopy* 17 (8): 1228–30.

Hruby, Gregory W., Franzo C. Marruffo, Evren Durak, Sean M. Collins, Phillip Pierorazio, Peter A. Humphrey, Mahesh M. Mansukhani, and Jaime Landman. 2007. “Evaluation of Surgical Energy Devices for Vessel Sealing and Peripheral Energy Spread in a Porcine Model.” *Journal of Urology* 178 (6): 2689–93.

Kelman, C. D. 1967. “Phaco-Emulsification and Aspiration. A New Technique of Cataract Removal. A Preliminary Report.” *American Journal of Ophthalmology* 64 (1): 23–35.

Kim, F. J., M. F. Jr. Chammas, E. Gewehr, M. Morihisa, F. Caldas, E. Hayacibara, M. Baptistussi, F. Meyer, and A. C. Martins. 2008. "Temperature Safety Profile of Laparoscopic Devices: Harmonic ACE (ACE), Ligasure V(LV), and Plasma Trisector (PT)." *Surgical Endoscopy* 22 (6): 1464–69.

Koch, Christian, Thomas Friedrich, Frank Metternich, Andrea Tannapfel, Hans P. Reimann, and Uwe Eichfeld. 2003. "Determination of Temperature Elevation in Tissue during the Application of the Harmonic Scalpel." *Ultrasound in Medicine & Biology* 29 (2): 301–9.

Landau, Lev D., and Evgeny M. Lifshitz. 1986. *Theory of Elasticity*. Oxford: Pergamon.

Lee, Sang J., and Ki H. Park. 1999. "Ultrasonic Energy in Endoscopic Surgery." *Yonsei Medical Journal* 40 (6): 545–49.

Majaron, B., P. Plestenjak, and M. Lukac. 1999. "Thermo-Mechanical Laser Ablation of Soft Biological Tissue: Modeling the Micro-Explosions." *Applied Physics B* 69 (1): 71–80.

Meltzer, R. C., D. M. Hoenig, C. A. Chrostek, and J. F. Amaral. 1994. "Porcine Seromyotomies Using an Ultrasonically Activated Scalpel." *Surgical Endoscopy* 8: 253.

Potter, Merle C., and Craig W. Somerton. 1993. *Theory and Problems of Engineering Thermodynamics*. New York: McGraw Hill.

Sankaranarayanan, Ganesh, Rajeswara R. Resapu, Daniel B. Jones, Steven Schwaitzberg, and Suvranu De. 2013. "Common Uses and Cited Complications of Energy in Surgery." *Surgical Endoscopy* 27 (12): 4758.

Stull, Daniel R. 1947. "Vapor Pressure of Pure Substances. Organic and Inorganic Compounds." *Industrial & Engineering Chemistry* 39 (4): 517–40.

Wallace, Duane C. 1972. *Thermodynamics of Crystal*. Mineola, New York: Dover Publications, Inc.

Wiksell, Hans, Harvey Martin, Hugh Coakham, Anders Berggren, and Sara Westermark. 2000. "Miniaturised Ultrasonic Aspiration Handpiece for Increased Applicability." *European Journal of Ultrasond* 11 (1): 41–46.

Wolfe, Bruce M., Barry N. Gardiner, Barbara F. Leary, and Charles. F. Frey. 1991. "Endoscopic Cholecystectomy: An Analysis of Complications." *Archives of Surgery* 126 (10): 1192–96.